Smart Drivers for Online Diagnosis of Electrostatic MEMS Actuators

Norbert Dumas, Laurent Latorre, Frédérick Mailly, Pascal Nouet

HAL Id: lirmm-00494515

https://hal-lirmm.ccsd.cnrs.fr/lirmm-00494515v1

Submitted on 23 Jun 2010

Smart Drivers for Online Diagnosis
of Electrostatic MEMS Actuators

N. Dumas, L. Latorre, F. Mailly, and P. Nouet, *Member, IEEE*

Abstract—This paper introduces the design of High-Voltage CMOS drivers for Electrostatic MEMS switches. In order to perform online diagnosis, the proposed architecture implements a dedicated circuitry that can detect the pull-in event. This way, stuck or broken switches are identified during operation. The pull-in event corresponds to a rapid change in the actuation capacitance thus producing a current peak during actuation. The idea is therefore to measure the charging current, using a differential method that cancels the effects of any parallel parasitic capacitance.

Index Terms— MEMS, CMOS, Electrostatic Actuator, Switch, Diagnosis

I. INTRODUCTION

AFTER years of continuous development and improvement, MEMS based electrostatic switches have become quite popular. They are now considered for various applications related to RF telecommunications where they advantageously replace the traditional PIN diodes as switching components, due to their unbeatable low insertion loss. Although much works have been done to improve MEMS switches reliability in the past years, the design of high added-value systems integrating such devices is not considered without some level of robustness against possible MEMS failure. This study is part of a project that target the design of reflect arrays antennas for telecom applications. In this application, thousands of MEMS switches are embedded into RF cells to open or short RF paths so that a continuous phase shift is achieved between incident and reflected waves. As different switches configurations may achieve the same phase shift, the architecture features an intrinsic redundancy so that alternate RF path may be used if non-working MEMS are well identified [1]. Moreover, a huge quantity of MEMS is used in a small surface, so that the control and driving circuitry, including the diagnosis functionality, must be integrated into small ASICs.

The proposed diagnosis approach is non-invasive from a RF point of view since RF path is not directly altered. It is based on the monitoring of the actuation current as used in [2] or [3] and thus only concerns the actuation circuitry. Note that the quality of the contact (either resistive or capacitive) is not monitored using this method.

II. SWITCH MODELING & SIMULATION

A. Device Architecture

This study addresses generic MEMS actuators or switches. It is only assumed that the actuation is based on electrostatic force in a parallel plate capacitor. The contact nature can be resistive or capacitive, using both serial or shunt configuration. For the simulations however, the pseudo-realistic case sketched in Fig. 1 is considered. It represents basic capacitive shunt architecture, which is very common in RF applications. The function of the switch is to connect two planes together in order to provide a path for the RF waves into the patch. The moving part of the switch is a metal cantilever beam attached (both mechanically and electrically) to a ground plane. It is actuated by means of a large bottom electrode which is positively biased. When actuated, the cantilever beam lands on a thin dielectric layer thus connecting the two planes through the capacitor C_{RF}. Since the thicknesses of the planes is greater than the thickness of the actuation electrode, the air gap between the cantilever and the actuation electrode never closes, preventing the device from known reliability issues associated with high electric fields in dielectrics. The price to pay is a higher actuation voltage and a lower ratio $C_{Act,up}/C_{Act,down}$ which makes the use of C_{Act} measurement more challenging for the diagnosis, as it will be developed later on in this paper. In addition, the parasitic capacitor C_P that results from the routing of the actuation electrode makes the measurement even more complicated.
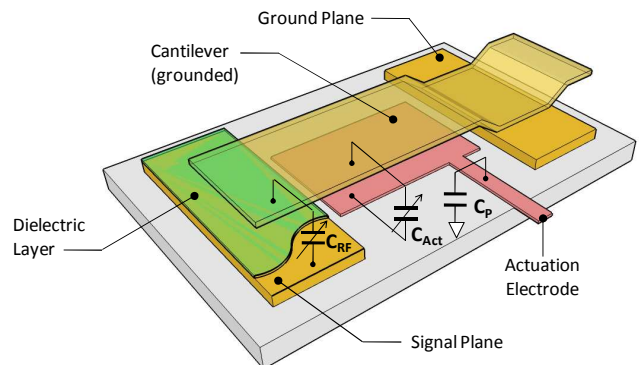

Figure 1. Structure of the MEMS switch under consideration.

B. Modeling

According to Fig. 2, the switch model is based on a spring-mass-damper system (kMD), translating along the vertical axis. The mass displacement z is controlled by an electrostatic actuator made of two parallel plates of surface S_A , separated by an initial gap g_0. Assuming that the bottom electrode is covered by a dielectric layer of thickness t_{ox} and of relative permittivity ε_r, the resulting capacitance between the two electrodes is given by:

$$C_{Act} = \frac{\varepsilon_0 S_A}{g_{eff}} \qquad (1)$$

where g_{eff} is the effective gap calculated by taking into account the two serial capacitances:

$$g_{eff} = z - t_{ox} + \frac{t_{ox}}{\varepsilon_r} \qquad (2)$$

The switch travel is practically hard-limited by the signal plane height. In order avoid convergence troubles within the simulator a squeeze-film damping effect is modeled into a so-called limiter block. This somehow makes the landing of the beam onto the finger surface smoother. Within a short range above the finger surface, the limiter acts in force-source mode and the squeeze film effect is modeled by an additional damping force given by:

$$F_L = \alpha \left(\frac{\eta S_F}{z - stop} \right) \dot{z} \qquad (3)$$

where η represent the air viscosity in Pas.s, S_F is the overlap surface between the bridge and the finger and α an exaggeration factor (set to 1 by default). If the conditions $z \approx stop$ and $\dot{z} \approx 0$ are reached, the limiter switches to position-source mode and holds the bridge at $z = stop$ as long as the electrostatic actuator forces the cantilever down.
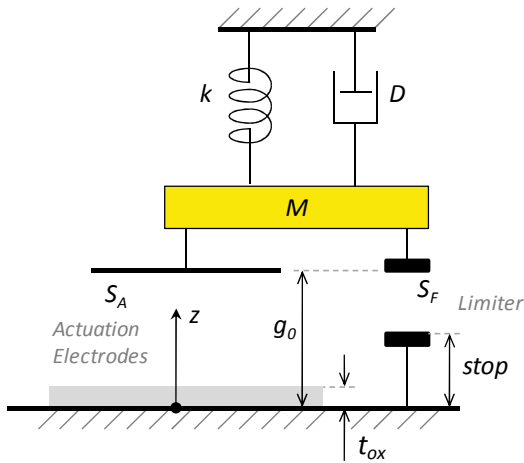
Fig. 3 shows the straightforward implementation of this model under Cadence®. Each part of the model is described using the proprietary Verilog-A language. The discipline *kinematic* is used to represent the z node. Using this discipline, the "across" quantity (same as voltage) represent the vertical position of the bridge, while the "through" quantity (same as current) represents the forces. Forces equilibrium of on node z is therefore a direct application of Kirchhoff's circuit laws. Table I summarizes the model parameters used in following simulations for further reference.
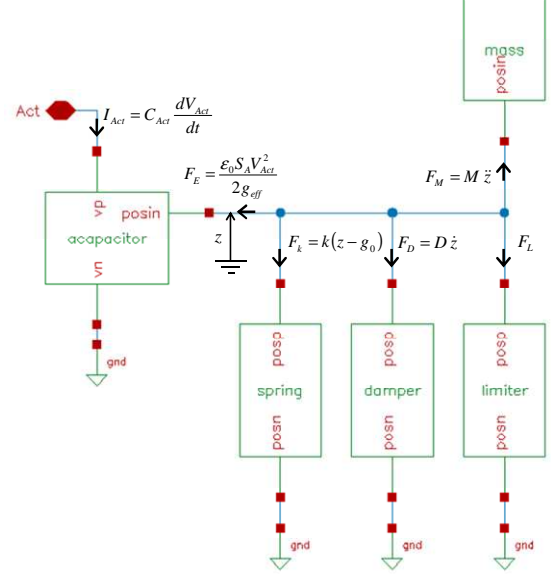

Figure 3. Model implementation within Cadence®.

TABLE I
ELECTROSTATIC SWITCH MODEL PARAMETERS

Cell	Symbol	Quantity	Value
acapacitor	S_A	Actuation Electrode Surface	100×10^{-9} m²
	ε_0	Abs. Permittivity	8.85×10^{-12} F.m^{-1}
	ε_r	Bottom dielectric relative permittivity	3.9
	t_{ox}	Bottom dielectric thickness	1µm
spring	k	Spring Constant	0.5 N.m^{-1}
	d_0	Initial gap	17µm
mass	M	Mass	1×10^{-10} kg
damper	D	Damping Factor	5×10^{-6} N.m^{-1}s^2
limiter	sflayer	Gap for squeeze-film damping action	0.5µm
	η	Air viscosity	18×10^{-6} Pas.s
	S_F	Finger overlap surface	25×10^{-9} m²
	stop	Finger height	2.65µm

Figure 2. Switch model.

III. SMART DRIVER DESIGN

The primary function of the driver is to provide the actuation voltage V_{Act} that is close to 46V in our case. For this, the High-Voltage (HV) 0.35µm CMOS technology (h34b4c3) from Austria MicroSystems (AMS) was chosen to develop the integration of such drivers in the context of a multiple channels chip. The design of the basic driver stage is addressed first. Then two approaches are proposed to upgrade the driving circuitry with a diagnosis capability.

A. High-Voltage Driver

The challenge when designing a HV driver is to combine the low voltage level of the control circuitry (typically 3.3V) with the higher voltages that bias the output stage (50V). In this study, it was assumed that only two external supply voltages were available: a low 3.3V and a high voltage supply that may vary from 20V to 50V to adapt various switch pull-in conditions.

The proposed driver is shown in Fig. 4. It is based on a pair of HV transistors Q_3 and Q_4. In this configuration, the gate of Q_4 can be directly driven by the low-voltage levels (0-3.3V). The gate of Q_3 must be driven between V_{CC} and a lower voltage that turns Q_3 on, while keeping the magnitude of V_{GS3} within 20V which is a technological constraint. This condition is ensured by the level-shifter stage made of Q_1, Q_2 and V_b. When input is 0, Q_2 is off. There is no current flowing in the level-shifter and V_{GS3} is 0. When input is 3.3V, Q_2 is turned on. The current flowing in the level shifter is regulated by the voltage drop across R_1 so that $V_{GS1} \approx -V_{tp} \approx -1,7V$. The voltage drop V_b is designed to be about 10V (50% of the 20V limit). It is implemented by means of few diode-mounted transistors in series, biased by a resistive load tied to the ground. Doing-so ensures that V_b stays constant for a wide range of supply voltage. It finally comes that the voltage on the gate of Q_3 in on-state is close to $V_{CC}-V_b+V_{tp} \approx 41.7V$. Note that the static consumption of the driver is here mainly determined by R_1 whose value is practically restricted by its cost in term of silicon area.
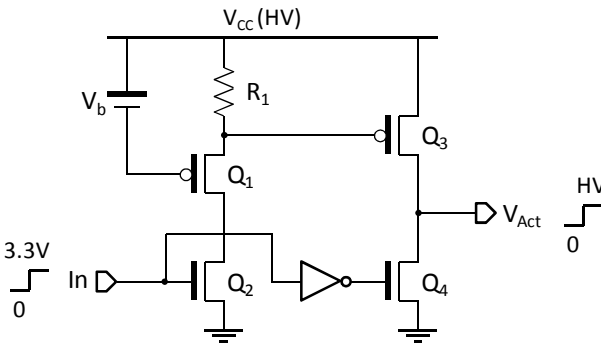

Figure 4. Structure of the HV driver.

B. Diagnosis Principles

Fig. 5 illustrates the transient response of the switch to an actuation pulse. It is obtained by the simulation of the HV driver previously described together with the switch model and a RC network (R_{ser}=1MΩ and C_{par}=5pf) representing a rather bad case for the routing. As mentioned before, the diagnosis approach must not interfere with the RF path. Fortunately, the switch pull-in produces a distinctive actuation current profile which is a good start for an investigation.

The driver output is turned on at t_0=0, providing an almost instant and stable 40V voltage for V_{Act}. The transient current then exhibits a first peak corresponding to the charge through R_{ser} of the capacitance $C_{par}+C_{Act,up}$. The charge is almost completed when V_{cap} reaches its final value of 40V ($t_1 \approx 30$µs) and before the cantilever starts its travel. At t_2=75µs, the cantilever gets close to its lower position producing a fast increase of C_{Act}. This causes a new small current overshoot corresponding to the charge of $\Delta C_{Act}=C_{Act,down}-C_{Act,up}$. Note that during this charge, the V_{Cap} voltage exhibits a small notch that can be neglected. Finally, all signals become stable after t_{end}=150µs.
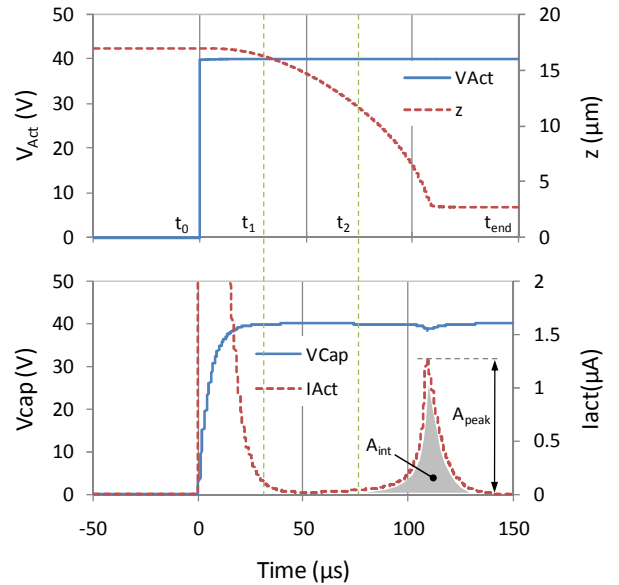

Figure 5. Transient simulation of an actuation event.

Since the second current peak will not occur in the case of broken or stuck MEMS, it makes sense to develop a diagnostic strategy based on the measurement of the actuation current. An obvious method would be the simple measurement of the amplitude of the second overshoot (A_{peak}), however the peak amplitude strongly depends on the routing parameters (R_{ser}, C_{par}) that may vary in a significant range. This is shown by the simulation in Fig. 6.a, where A_{peak} varies by 120% with the routing parameters. On the other hand, the amount of electric charges transferred in the electrostatic actuator when C_{Act} changes from $C_{Act,up}$ to $C_{Act,down}$ is relatively insensitive to

routing parameters. Fig. 6.b shows that the current integral (A_{int}) measured within the time window corresponding to the second current peak only varies by 4% for the same routing parameters range. As a consequence, a diagnostic approach based on the actuation current integration seems more appropriate in our case.
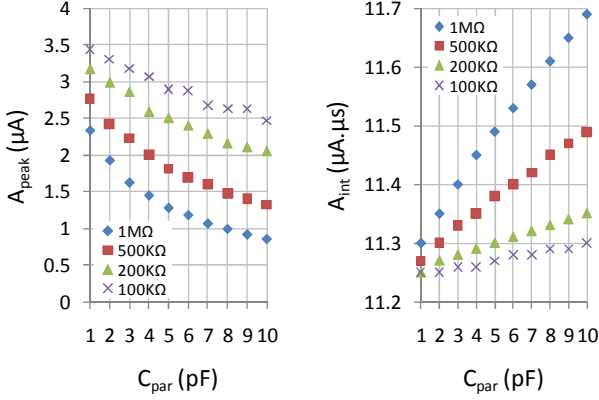

Figure 6. a-(left) Variation in amplitude of the second actuation current peak as a function of routing parameters. b-(right) Variation of the actuation current integral during the second peak.

The total amount of charges stored in C_{par} and C_{Act} during the whole actuation process does not depend on R_{res} and writes:

$$q(t) = V_{Act}(t)\left(C_{par} + C_{Act}(t)\right) \qquad (4)$$

Looking at the actuation current, we have:

$$i_{Act}(t) = \frac{dq(t)}{dt} =$$
$$\left(C_{par} + C_{Act}(t)\right)\frac{\partial(V_{Act}(t))}{\partial t} + V_{Act}(t)\frac{\partial(C_{Act}(t))}{\partial t} \qquad (5)$$

The second spike of current is caused by the second term of Eq. 5 when the actuation voltage is constant and the capacitance changes. As the derivative of the actuation voltage is null during the second spike, the integration of the actuation current from the beginning of the second spike t_2 to t_{end} results in:

$$\int_{t_2}^{t_{end}} i_{Act}dt = \int_{t_2}^{t_{end}} V_{Act,end}\frac{d(C_{Act}(t))}{dt}dt = V_{Act,end}\Delta C_{Act} \quad (6)$$

With:
$$\Delta C_{Act} = C_{Act,end} - C_{Act,0} = C_{Act,down} - C_{Act,up}$$

Eq. 6 clearly expresses that the result of integrating the actuation current during the second spike does not depend on the parasitic capacitance. However, it is valid only if the two spikes can be well separated. It implies that the time constant of the first spike, i.e. $R_{res} \times C_{par}$, should be much lower than the time response of the switch.

C. Smart- Driver Architecture #1

The first improved version of the HV driver presented above is depicted in Fig. 7. In this circuit, the actuation current is mirrored into the capacitor C_{int} so that the voltage across C_{int} represents the integration of I_{Act}. A cascode mirror configuration, with a copy ratio $\beta = W_{Q6,Q8}/W_{Q5,Q7}$, has been preferred to improve the V_{DS} matching of the pair Q_5/Q_6 and thus guaranty a better accuracy of the copy. Transistor Q_9 is used to initialize the integrator state and then start the integration process upon falling edge of the *Reset* control input. Note that the gate Q_9 is associated with dummy transistors (not represented) to minimize integration errors due to charge injection.
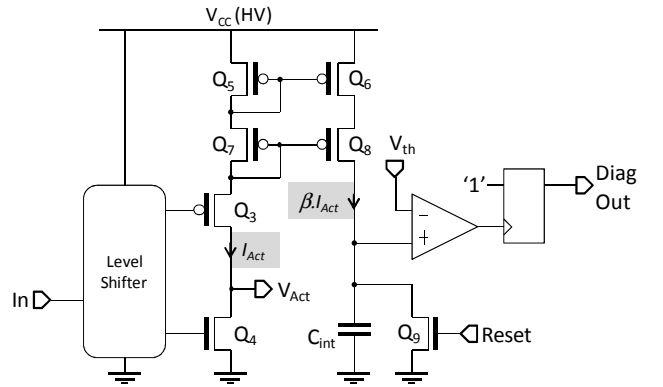

Figure 7. Structure of the HV driver with Actuation Current integrator.

If the voltage across C_{int} reaches V_{th}, a '1' is stored in the latch meaning a successful commutation of the switch, otherwise the diagnosis output is '0'. The independent control of the *Reset* pin allows the integration process to start anytime.

Two strategies have been investigated: If the MEMS time constant is short, or uncertain, the integration may start from t_0. In that case, the total actuation current is summed up in the integrator and the result depends strongly on the parasitic capacitance. Therefore, the parasitic capacitance should be known in order to make the diagnosis. Otherwise, if the MEMS time constant is long and well characterized, the integration may start from t_2 so that only the current associated with the pull-in event is accumulated. This second method has been validated with results reported in [3].

D. Smart-Driver Architecture #2

The previously proposed method requires the good knowledge of the switch dynamic behavior, which must feature a slow-enough, predictable and stable time response to detach the pull-in from the charge of the parasitic capacitance. If these conditions are not met, a different approach to eliminate the effects of the routing parameters is necessary. A possible solution is proposed with the architecture shown in Fig. 8.
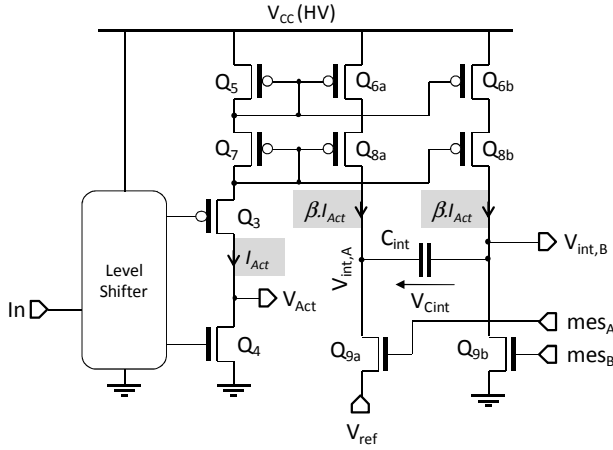
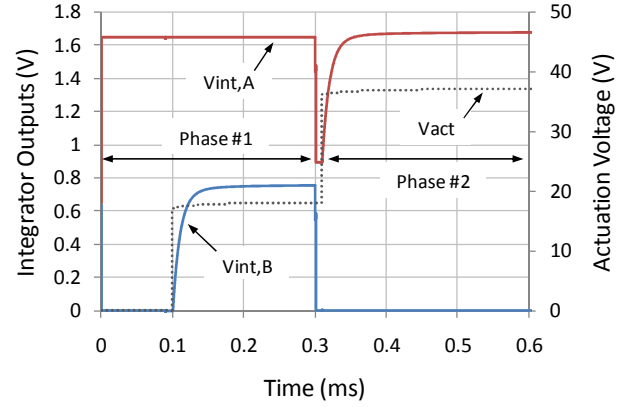Figure 8. Structure of the HV driver with a Differential Actuation Current integrator.

Figure 9. Simulation of the HV driver diagnosis sequence without MEMS.
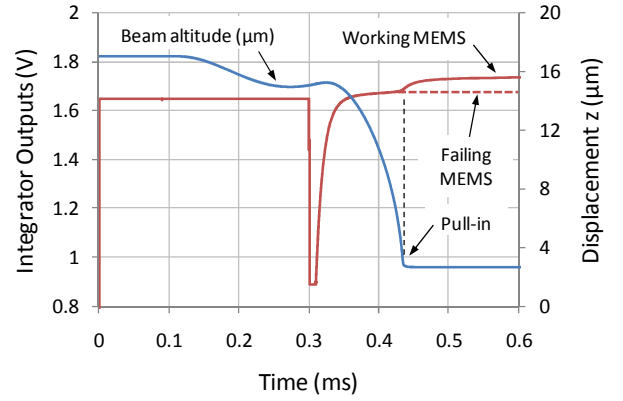
Figure 10. Simulation of the HV driver diagnosis sequence with working MEMS.

The measurement sequence start with an initialization of the charge in C_{int} by turning on both Q_{9a} and Q_{9b} so that $V_{Cint} = V_{ref}$. During phase #1, V_{cc} is set to provide only half of the final actuation voltage V_{Act} at the driver output, Q_{9b} is turned off and the driver is activated (In='1'). The actuation current is summed up in C_{int}. After the integration time, and assuming that the driver output is below the pull-in voltage the voltage, $V_{int,B}$ is given by:

$$V_{int,B} = \frac{\beta}{C_{int}} \frac{V_{Act}}{2} \left(C_{par} + C_{Act,up} \right) \qquad (7)$$

During phase #2, the transistor Q_{9a} is turned off, and Q_{9b} is closed to connect the node $V_{int,B}$ to ground. At this moment, the voltage $V_{int,A}$ is:

$$V_{int,A} = V_{ref} - V_{int,B} \qquad (8)$$

V_{CC} is now adjusted to make the driver outputs V_{Act} so that another $V_{Act}/2$ voltage step is applied on the switch. The pull-in occurs and then after another integration period, $V_{int,A}$ becomes:

$$V_{int,A} = \left(V_{ref} - V_{int,B} \right) + \frac{\beta}{C_{int}} \frac{V_{Act}}{2} \left(C_{par} + C_{Act,down} \right)$$
$$V_{int,A} = V_{ref} + \frac{\beta}{C_{int}} \frac{V_{Act}}{2} \Delta C_{Act} \qquad (9)$$

In summary, the amount of current charging C_{par} is summed up in C_{int} during the first $V_{Act}/2$ step, and then subtracted during the second $V_{Act}/2$ step, leaving the integrator output with an image of the ΔC_{Act} charge only.

The complete sequence shown in Fig. 9 with no MEMS connected to the driver. Because $\Delta C_{Act} = 0$ in this case, the diagnosis output ($V_{int,A}$) is V_{ref} at the end. The simulation is performed with $R_{ser}=1M\Omega$, $C_{par}=10pF$, $\beta=1/16$ and $C_{int}=15pF$. With $V_{cc}=40V$, the actuation voltage is roughly $V_{act}=37.2V$. According to Eq. (7), the voltage $V_{int,B}$ after phase #1 reaches 775mV, which is verified by the simulation.

In Fig. 10, the simulation is performed with the electrostatic switch connected to the driver. The change in capacitance during the pull-in produces an increase of $V_{int,A}$ of about 60mV. According to Eq. (9), it corresponds to a change in capacitance of $\Delta C_{Act} = 770fF$. This value is in the range of expected change according to the model parameters reported in table I. The robustness of the approach against routing parameters (R_{ser}, C_{par}) has been investigated with results reported in Fig. 11. It appears that for each case, the working MEMS produces a result well distinguishable from the result obtained with a broken switch. Note that the result strongly depends on the ability to set the correct V_{cc} that produce a precise $V_{act}/2$. In this simulation, this V_{cc} is set manually to 21V. Practically, this half-supply voltage can be generated on-chip within a dedicated circuit that will address process variations and better separation between working and failing case is then expected.
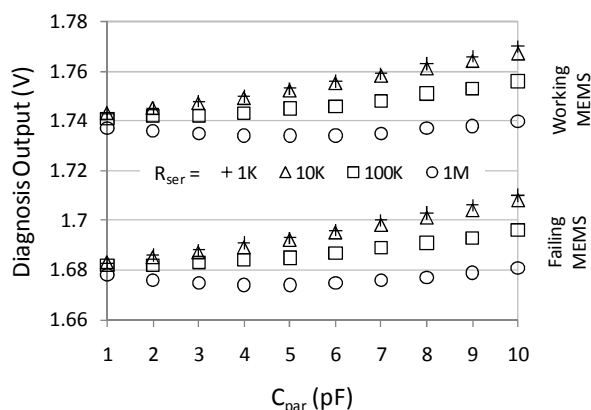
Figure 11. Comparison of diagnosis output for different routing parameters (R_{ser}, C_{par}) with working and non-working MEMS.

IV. EXPERIMENTAL RESULTS

A test chip including 18 driver channels has been fabricated using the High-Voltage 0.35µm CMOS technology from Austria Microsystems. The chip has been connected to both fixed capacitors and MEMS switches (Fig. 11).
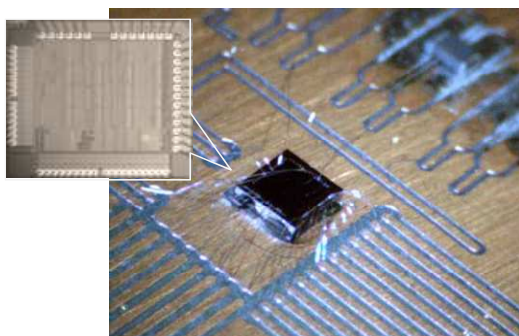

Figure 11. Custom PCB for the assembly of the test chip with fixed capacitors and MEMS switches.

First experiments have demonstrated that the driver part operates as specified with MEMS switches regarding actuation. For the characterization of the diagnosis function, fixed capacitors representing C_{par} have been initially connected to the driver without MEMS. For three values of C_{par}, the diagnosis output ($V_{int,A}$) voltage is presented in Fig. 12. The corresponding sensitivity is 3.6mV/pF, which is low enough to consider that the effect of C_{par} is correctly rejected (rejection ratio is about 30).

Fig. 13 displays the output of the diagnosis circuit during a MEMS actuation. Qualitatively, the waveform is very similar to the one obtained by simulation (Fig. 10). An additional 25mV is brought across the integrator capacitor (C_{int}) during pull-in, corresponding to a 260fF change in the MEMS actuator capacitance.
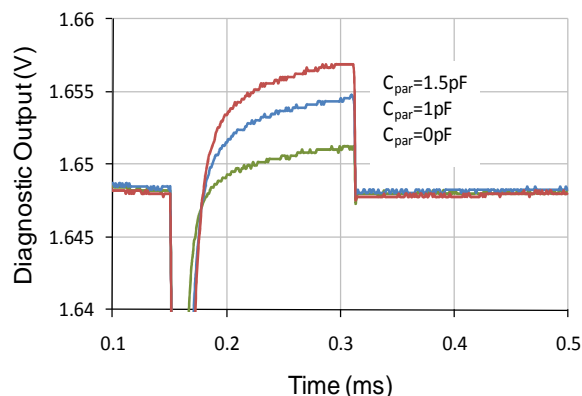

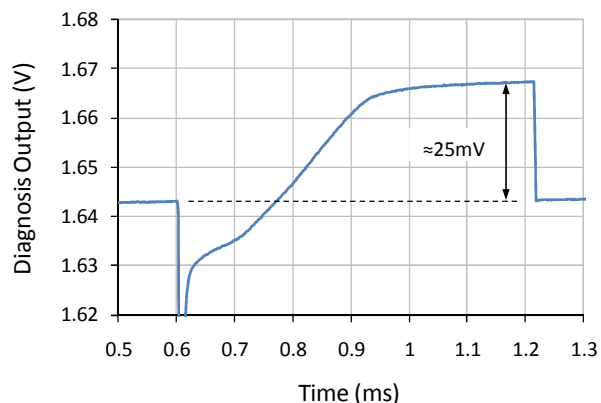Figure 12. Measured diagnosis output voltage, for three values of Cpar, without MEMS

Figure 13. Measured diagnosis output voltage with a MEMS.

V. CONCLUSION

This paper introduces the design of High-Voltage drivers for MEMS electrostatic relays with diagnosis capability. The diagnosis is based on the measurement of the actuation current. A differential measurement technique that cancels the effect of serial resistance and parallel parasitic capacitance is proposed and validated by both simulations and experiments.

ACKNOWLEDGMENT

REFERENCES

[1] H. Salti, E. Fourn, R. Gillard, H. Legay, H. Aubert, "MEMS breakdown effects on the radiation of a MEMS based reconfigurable reflectarray", 3rd European Conference on Antennas and Propagation (EuCAP'09), Berlin, 23-27 March 2009, pp. 3738 – 3741.

[2] B. Caillard, Y. Mita, Y. Fukuta, T. Shibata, and H. Fujita, "A highly simple failure detection method for electrostatic microactuators: application to automatic testing and accelerated lifetime estimation," IEEE Transactions on Semiconductor Manufacturing, vol. 19, no. 1, pp. 35–42, 2006.

[3] W. Merlijn van Spengen, R. Puers et. al., "Experimental Charaterization of Stiction Due to Charging in RF MEMS", International Electron Devices Meeting (IEDM), 2002, pp. 901-904.

[4] N. Dumas, L. Latorre, F. Mailly, P. Nouet, "Design of a Smart CMOS High-Voltage Driver for Electrostatic MEMS Switches", Design Test Integration & Packaging of MEMS/MOEMS (DTIP'10), 5-7 May, Seville, Spain, 2010.